

ATTITUDE AND HEADING REFERENCE SYSTEM FOR AN INTEGRATED STAND-BY DISPLAY INCORPORATING SOLID STATE SENSORS

M. Carminati¹, G. Ferrari¹, M. Sampietro¹ and R. Grasseti²

¹ Politecnico di Milano, Dipartimento di Elettronica e Informazione
P.za Leonardo da Vinci 32, I-20133 Milano

² Logic S.p.A. - Via Galileo Galilei 5, Cassina de' Pecchi, Milano
Italy

OVERVIEW

The design of a compact solid state attitude and heading reference systems (AHRS) is currently a challenging task, common to the development of navigation systems for UAV's (Unmanned Aerial Vehicles), general aviation and high performance stand-by instruments, not to mention other terrestrial and submarine vehicles. The AHRS presented here is to be incorporated in a stand-by display, in order to turn it from a repeater display into a self-contained, autonomous and complete guidance system, composed by internal assemblies measuring heading, attitude and air data. We shall illustrate the system architecture, sensor selection criteria, analog signal conditioning, digital elaboration stages and calibration procedures, highlighting design choices and trade-offs. The compass is tilt compensated and therefore based on a triad of orthogonal magnetoresistive sensors. The attitude subunit is based on MEMS inertial sensors. Our approach for attitude determination, illustrated in the context of a brief literature review, consists in the use of a triad of rate gyros as main attitude sensors whose diverging error is corrected by the complementary gravimetric attitude estimate provided by a triad of accelerometers. The data fusion algorithm is based on a 9-state extended Kalman filter. The results of laboratory tests of the demo-prototypes are presented. The angular resolution of the AHRS is better than 0.1° and the static accuracy is 0.5° over the entire thermal range. Those performances are well within the desired specifications and have been experimentally verified.

1. STAND-BY DISPLAY

1.1. Introduction

Stand-by instruments are compulsorily installed in the cockpit to provide the pilot with redundant guidance information that must guarantee a safe landing in case of failure of main systems. Therefore such units have an autonomous power supply and contain independent sensors to measure basic flight parameters. The instrument is constantly active and must display correct information that can be used as a cross-check of main navigation systems also in the absence of breakdowns.

Basic information displayed by this system are heading, roll and pitch angles, barometric altitude, air-speed, vertical speed and yaw rate. In the past, each singular flight parameter was measured and displayed by a different electromechanical instrument. Today, following the modern design trends^[1] in development of avionic

systems, the state of the art is represented by ESIS (Electronic Stand-by Instrument Systems) i.e. fully electronic units that concentrate the data in a single 3" AMLCD (Active Matrix Liquid Crystal Display) as illustrated in FIG 1.

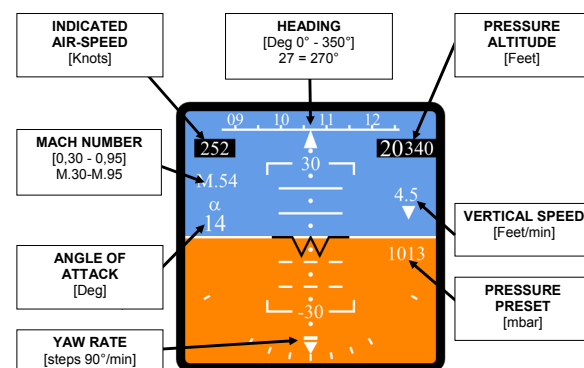


FIG 1. AMLCD 3" Air Transport Instrument (ATI) display with fundamentals flight parameters.

The main advantages offered by 3 ATI^[2] ESIS, beyond improved performances with respect to previous instruments, are extreme compactness, ruggedness, personalization, ergonomics and ease of installation and maintenance. They can also interface through standard busses with other systems in order to enrich the presentation of flight parameters with auxiliary navigation information.

The research project presented here has been carried on jointly by the Department of Electronics and Information Technology of Politecnico di Milano and Logic S.p.A., an avionics Italian company. The target of this project, not yet concluded, is the thorough design of the system. In particular we present here the critical issues involved in the design process of the compass and the attitude estimation subunit that together constitute the AHRS.

1.2. System Distributed Architecture

To realize a truly electronic system, solid state sensors are needed and a strap-down^[1] approach must be adopted. Thus, sensors are rigidly mounted in a fixed orientation with respect to the aircraft axes and the necessary mechanization equations are solved in the digital domain by a dedicated processor.

Most sensors, analog signal conditioning stages and

digital circuitry are housed inside the display chassis and must therefore satisfy very stringent volume constraints. Only two subunits, for different reasons, are separate from the main unit. The magnetometer is remotely installed in a place where electromagnetic interferences and magnetic distortions are minimal, typically near the tail. Consequently a 20 meter dedicated bidirectional digital line (RS-422) connects the magnetic sensor cluster to the central system. Data travel in digital form for a more robust noise rejection and bit rate is not critical due to the low frequency heading visualization.

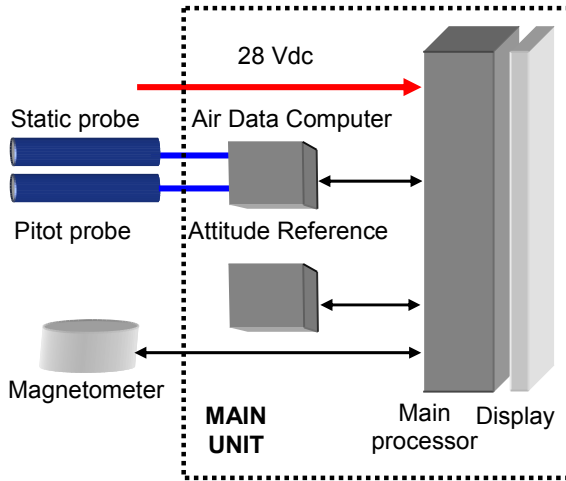


FIG 2. Distributed functional architecture of the system.

The air data computer should also be detachable, in order to be installed in a more convenient position with respect to the pipes of pressure probes. Thus, it's clearly evident that another advantage of modern fully electronic implementations is the flexibility of optimally displacing remote units away from the glass cockpit. The resulting distributed architecture is schematically pictured in FIG 2.

1.3. System Specifications

The minimal target performances of the AHRS are listed in TAB 1.

Angular Resolution	0.1°
Static Angular Accuracy	±0.5°
Dynamic Angular Accuracy	±2°
Heading Displaying Time Constant	250ms
Attitude Data Refresh Interval	20ms
Min. Operating Temperature	-40°C
Max. Operating Temperature	71°C
Max. Angular Rate	400°/s

TAB 1. AHRS minimal target performances

Static accuracy refers to a requirement in levelled

conditions while dynamic implies the presence of manoeuvres that can reach the maximum angular rate and maximum linear acceleration of 5g, 3g and 10g respectively for x, y and z axis.

2. MAGNETIC COMPASS

2.1. Solid State Magnetic Field Sensors

The Earth's magnetic field has an intensity ranging from 0.2 to 0.5 Gauss. Due to the intimate relation existing between electrical and magnetic phenomena, there are plenty of electronic magnetic sensors covering this range. We concentrated our analysis on solid state sensors for the clear advantages in terms of cost, ruggedness and volume. The available sensors can be grouped in 4 technological families: magnetoinductive^[3], Hall effect^[4], micro-fluxgate^[5] and magnetoresistive^[6].

The best performances (sensitivity, resolution and bandwidth) are offered by AMR (Anisotropic Magneto Resistance) sensors, whose technology is now well consolidated^[7]. The same cannot be said about the other classes of sensors that are still under development, like Hall effect sensors that, being the only type of sensors truly compatible with standard CMOS processes, appear very promising. The magnetoresistive effect^[8] consists in the change of resistivity of a slab of a ferromagnetic material (*Permalloy* - an alloy of iron and nickel) proportionally to the magnetic field externally applied along the sensitivity axis. Another important feature is the extended thermal operating range (-54°C ÷ +71°C) that AMR sensors can guarantee. In fact, the magnetometer is remotely located in a thermally uncontrolled part of the fuselage and it must satisfy accuracy requirements all over that range.

2.2. Architecture and Calibration

Heading (ψ) can be calculated from the horizontal components of the Earth's magnetic field H_y and H_x as:

$$(1) \quad \psi = \text{atan}\left(\frac{H_y}{H_x}\right)$$

when the aircraft is levelled. In order to be tilt-compensated, i.e. to provide accurate heading indication during manoeuvres, the compass must be based on a 3D measurement of the magnetic vector and on an instantaneous knowledge of attitude. So, by means of the on-line estimate of roll and pitch angles provided by the attitude unit the projections of the magnetic field measured by the orthogonal triad of strap-down sensors are rotated back into the horizon plane.

Compass calibration is necessary to compensate for magnetic distortion caused by hard and soft irons present on board. After installation, the calibration is executed through the swinging procedure in a dedicated airport emplacement whose orientation is precisely known. The error $\delta(\psi)$ is periodical with respect to heading angle and is fitted by an harmonic function, a Fourier polynomial arrested at the second term, as indicated in Eq. (2). The 5 coefficients $A - E$ can be identified from the recorded

heading values for steps of $10^\circ - 45^\circ$ at fixed orientations, through least squares method. It's important to underline that this procedure enables the contemporaneous removal of different errors: misalignment (constant term A), gain errors and cross-sensitivity.

$$(2) \delta(\psi) = \begin{bmatrix} A \\ B \\ C \\ D \\ E \end{bmatrix}^T \times \begin{bmatrix} 1 \\ \sin(\psi) \\ \cos(\psi) \\ \sin(2\psi) \\ \cos(2\psi) \end{bmatrix}$$

2.3. Offset and Thermal Drift Reduction

The analog signal conditioning stages of the 3 channels contain two peculiar topologies, both required to overcome the effects of the two dominant errors affecting this type of sensors. The main limitation to measurement accuracy is due to the sensor offset, caused by the unavoidable mismatch existing among the four magnetoresistive arms of the Wheatstone's bridge, present in each sensor. The effect of offset is contrasted by the use of a lock-in amplifier (FIG 3). In fact, thanks to the possibility of flipping^[9] the sensor output (i.e. inverting the sign of the sensor gain) by periodically changing of 180° the orientation of the Permalloy magnetic domains, with an intense bipolar current pulse, the signal can be modulated. In this way the error source is spectrally decoupled from the signal: the offset remains at DC while the signal is translated around a 1kHz carrier. So, through frequency selective filtering and demodulation an offset-free, SNR-improved, low frequency measurement can be obtained.

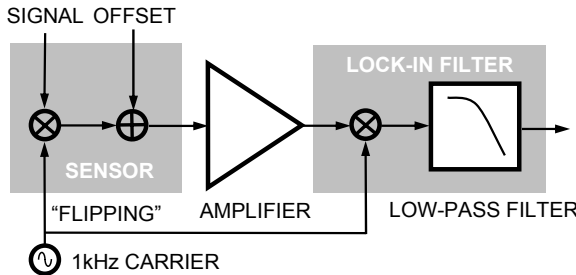


FIG 3. Basic principle scheme of lock-in synchronous filtering.

The second error source is the sensor sensitivity thermal drift. As shown in equation (1) heading depends upon the ratio of the measured components, so all the multiplicative coefficients get simplified and the estimate is independent on the modulus of Earth's magnetic field and sensor gain, as long as it is the same for the 3 channels. Due to a quite intense drift ($0.3\%/^\circ\text{C}$) a difference in temperature of a few degrees among them causes an error greater than the static accuracy requirements. This problem is faced by the solution of putting the sensor inside a sensor-actuator closed-loop (FIG 4). Being available an extra metal coil integrated in the chip that generates a local field along the sensitivity axis to be subtracted from the external field, it's possible to close a negative feedback loop by driving that coil with a current proportional to the sensor output signal. Doing that, the sensor is forced to operate in the origin of its characteristic, where the thermal sensitivity is minimum and the global transfer function depends on the feedback

actuator (the coil) which has better thermal stability. The intensity of the measured field is now indicated by the current needed to null it.

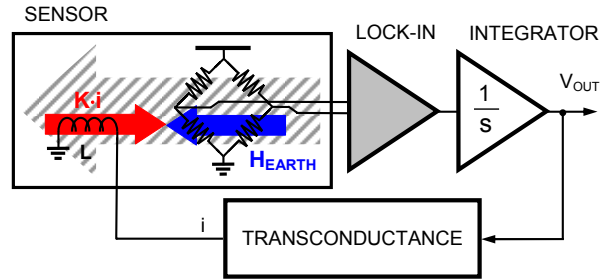


FIG 4. Block diagram of the magnetic feedback topology.

3. ATTITUDE ESTIMATION UNIT

3.1. MEMS Inertial Sensors

The need for compactness and low cost clearly addresses towards the choice of MEMS (Micro Electro Mechanical Systems) inertial sensors for the ESIS attitude subunit. In fact, the performance of those micromachined sensors are constantly improving, making them the proper choice not only for miniaturized UAV inertial navigation systems but also for stand-by instrumentation. The still existing gap between their raw performances and the system specifications can be reduced by multisensor approaches and powerful data fusion algorithms, able to optimally extract and blend information provided by clusters of sensors.

Selection criteria of inertial sensors (rate gyros and accelerometers) beyond supply voltage, operating range and bandwidth, are the performances expressed in terms of the incidence of undesired non-ideal error sources. In fact, the output voltage of a real micromachined inertial sensor sensing the measurand $M(t)$ can be written as:

$$(3) V_{out}(t) = S \cdot M(t) + b + n(t) + C(t)$$

where S is the sensor sensitivity, b the constant offset (or bias), n the superimposed zero-mean noise and the term C contains spurious cross-sensitivity effects. The impact of each term depends on the sort of signal elaboration and in this application the dominating factors are the offsets of the sensors and their variation with temperature.

3.2. Multisensor Attitude Estimate

The gyroscope is the principal available sensor for attitude measurement, also in MEMS domain. Being its output signal proportional to the angular rate (ω), to obtain the instantaneous angular tilt (θ) one should integrate it over time starting from a known initial condition θ_0 . In the single axis case:

$$(4) \theta(t) = \theta_0 + \int_0^t \omega(\tau) d\tau$$

while for both roll (φ) and pitch (θ) angles the differential equation which relates angular rates measured in the body-fixed reference system (ω_x , ω_y and ω_z) with attitude

angles time derivatives, expressed in the Earth-fixed frame, are:

$$(5) \begin{bmatrix} \dot{\varphi} \\ \dot{\theta} \end{bmatrix} = \begin{bmatrix} 1 & \sin \varphi \cdot \tan \theta & \cos \varphi \cdot \tan \theta \\ 0 & \cos \varphi & -\sin \varphi \end{bmatrix} \times \begin{bmatrix} \omega_x \\ \omega_y \\ \omega_z \end{bmatrix}$$

From those 2 non-linear coupled differential equations it's evident that:

- 1) in presence of 3D rotations it's impossible to operate with decoupled single-axis measurements, but both angles must be simultaneously calculated;
- 2) although the unknown angles are only 2, at least 3 orthogonal angular rate sensors are needed;
- 3) when pitch is equal to $\pm 90^\circ$ the roll derivate diverges.

The third property is intrinsic to the Euler angles attitude parameterization. It can be demonstrated^[10] the every minimal parameterization has at least one singularity. That is the reason why in most cases non minimal parameterizations are used such as quaternions or direction cosines. Beyond avoiding singularities, these parameterizations present a much more robust and stable numerical behaviour. Consequently we have adopted a non minimal parameterization.

The main problem involved in the use of gyros only is raised by the operation of integration itself. In fact, the accumulation of non-ideality induced errors causes an unbound divergence of attitude estimate. If the signal conditioning stages are properly designed, measurement errors are completely imputable to the sensors. The dominating error source are offset (bias) and noise. In fact the integration of a constant bias produces a linear output drift (ramp) while the integral of white noise (large bandwidth noise) is a random walk, whose standard deviation grows with the square root of time. There are two possible ways to solve this fundamental problem. The first consists in choosing high performance sensors so that, during a time equal to the maximum length of a mission, the accumulated error is inferior to accuracy requirements. The second way is more radical and allows for unlimited operational time. This approach is called multisensor^[11] and is based on the addition a corrective mechanism, typically a complementary sensors system that can periodically fix the diverging error of gyros. We have chosen the latter approach.

3.3. System Complementary Architecture

As a complementary source of information we chose the gravimetric attitude estimate. In fact, from the 3D measurement of the direction of gravity acceleration it's possible to obtain the tilt of the strap-down triad of accelerometers (A_x , A_y and A_z) with respect to the horizon, according to the formulas:

$$(6) \theta(t) = a \tan \left(\frac{-A_x}{\sqrt{A_y^2 + A_z^2}} \right)$$

$$(7) \varphi(t) = a \tan \left(\frac{A_y}{A_z} \right)$$

The main problem of such an accelerometer-based attitude measurement is that every dynamical acceleration impressed by maneuvers is superimposed to gravity and therefore affects the accuracy of the estimate. So this estimate is reliable only in static conditions, when no maneuvers take place and gravity is the dominant acceleration. Under the hypothesis that such moments of leveled attitude take place with a rate high enough to periodically reset the diverging error before it exceed the admitted range, this method is satisfactory. Furthermore, if we consider all dynamical spurious accelerations as a zero mean signal, by averaging over a sufficiently long period of time, we can extract from this low pass filtering a long term zero reference to be compared with gyros estimate. Thus the two sensor groups are complementary, in the sense that gyros provide an high frequency signal while the accelerometers slowly correct the estimate with a low frequency gravimetric reference. Consequently, the attitude estimation system is based on a cluster of sensors composed by a triad of accelerometers and gyros, in which the formers are used to measure only gravity while rejecting all other inputs, in an opposite fashion with respect to standard IMU's (Inertial Measurement Unit).

We have considered the possibility of tilting the triad of accelerometers as suggested in literature^[12] but simulations didn't show any performance improvement, against the considerable disadvantage of a much more complicate and bulky mounting. Furthermore, the final installation tilt of the ESIS in the cockpit can be different from zero and quite spread among different aircrafts. Thus, we chose to align the triad with the unit chassis. The correction for the alignment of the sensors cluster with aircraft axes is included in the static calibration procedure described in paragraph 4.4.

In order to cover the lowest part of the spectrum, the bandwidth of the accelerometers must include DC. Therefore the accelerometer offset directly affects the accuracy of measurements. By linearization of equations (6) and (7) it's possible to obtain an estimate of the impact of offset on angular static error. With a 10g full scale range accelerometer and 5V single supply voltage an error of 0.2° for the roll angle is due to 1.75mV and 1mV offset corresponding respectively to 7mg for y and to 4mg for x axis. MEMS accelerometers available on the market have offset about 10 times grater, that therefore must be calibrated for each single sensor of each single unit. In order to simplify the calibration procedure to only a one-point room temperature step, offset thermal drift must be faced. We chose to adopt a differential architecture for each single axis as depicted in FIG 5, measuring the difference between two sensors aligned in opposite directions. This solution imposes an undesired increase in cost and slightly in volume, due to the addition of three more accelerometers, but offers the important advantage that the global thermal drift is reduced significantly. In fact, if a single sensor has an output signal that can be expressed as:

$$(8) V_{out} = S_A \cdot A + V_{os}(25^\circ C) + k \cdot (T - 25^\circ C)$$

where S_A is the sensitivity, V_{os} is the offset voltage at room temperature ($25^\circ C$) and k is the thermal drift. The difference of two counter-aligned sensors becomes:

$$(9) V_1 - V_2 = 2S_A \cdot A + V_{os1} - V_{os2} + (k_1 - k_2)(T - 25^\circ C)$$

At 25°C the global offset is the difference of the two offsets (that can be even larger) but the resulting thermal drift is now equal to the mismatch existing between the singular drifts, typically at least an order of magnitude smaller than them. Thus, once calibrated at 25°C, the error induced by a temperature change equal to the entire operative thermal range causes an angular error within accuracy requirements, as illustrated in paragraph 4.4. Global measurement noise power increases of a factor 2 for the two sources are uncorrelated, while the signal doubles in amplitude so that the global SNR (Signal-to-Noise Ratio) is improved by a factor $\sqrt{2}$.

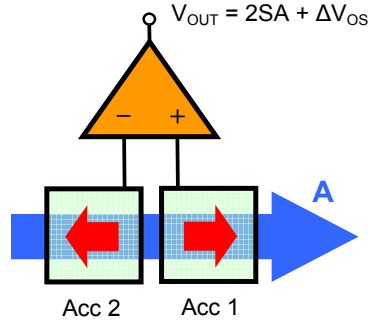


FIG 5. Differential configuration for each axis.

3.4. Data Fusion Techniques

After choosing the proper sensors, the most critical issue concerns the design of the fusion algorithm that will blend data acquired from both triads. As illustrated in FIG 6, in literature many approaches have been proposed; they can be grouped in three categories: Kalman filtering, complementary filtering and Whaba's problem^[13].

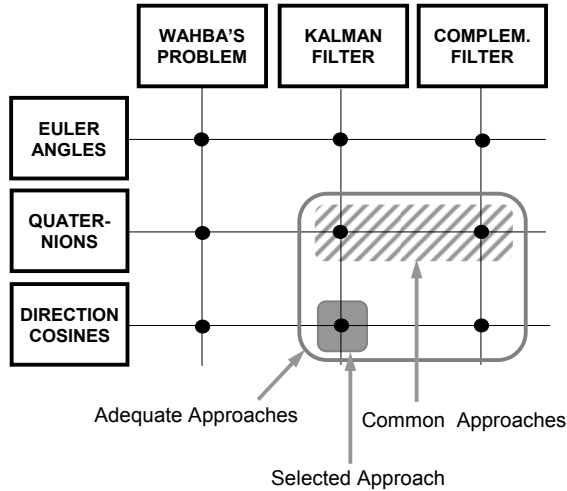


FIG 6. Matrix of possible combinations of commonly adopted parameterizations and data blending techniques.

We chose to implement a Kalman filter that represents the optimal solution^[14] to data blending problem. We discarded recursive algorithms (Whaba) for least squares estimate of attitude based on measurements of two known vectors (gravity and magnetic field) because they don't directly

take advantage of gyros, thus being prone to larger dynamical inaccuracies and require detailed information of geographical behaviour of such vectors. We also put aside complementary filters that, being time-invariant filters, offer worse performances.

As indicated in FIG 6, we selected direction cosines. After discarding Euler angles for the singularity problem, we have compared two non minimal parameterizations: quaternions and direction cosines. We opted for direction cosines, as suggested by Rhebinder^[15] because, when considering only roll and pitch, they show the same performances of more commonly used quaternions but with 3 parameters instead of 4.

3.5. The Extended Kalman Filter

The design of a Kalman filter implies a fundamental trade-off between dimension of state vector (and consequently degree of model detail) and computational burden. Very often the excessive computational load leads to suboptimal implementations that again fall in the family of time-invariant complementary filters. Therefore, we decided to start with a minimal dimension filter. Among the various errors we chose to track only the biases of gyros, that are definitely the dominating error source.

We adopted a tight-coupling approach^[14] feeding all acquired data directly to the Kalman filter, without any preprocessing operation or external integration step. According to this approach, the state vector includes 9 variables: attitude direction cosines (3 parameters), 3 angular rates (ω_x , ω_y , and ω_z) and 3 gyros biases:

$$(10) \begin{bmatrix} x_1 \\ x_2 \\ x_3 \\ x_4 \\ x_5 \\ x_6 \\ x_7 \\ x_8 \\ x_9 \end{bmatrix} = \begin{bmatrix} -\sin \theta \\ \cos \theta \cdot \sin \varphi \\ \cos \theta \cdot \cos \varphi \\ \omega_x \\ \omega_y \\ \omega_z \\ \delta_x \\ \delta_y \\ \delta_z \end{bmatrix}$$

Roll and pitch angles can be obtained from the first 3 variables through equations (6) and (7). The propagation matrix of direction cosines is:

$$(11) \begin{bmatrix} \dot{x}_1 \\ \dot{x}_2 \\ \dot{x}_3 \end{bmatrix} = \begin{bmatrix} 0 & \omega_z & -\omega_y \\ -\omega_z & 0 & \omega_x \\ \omega_y & -\omega_x & 0 \end{bmatrix} \times \begin{bmatrix} x_1 \\ x_2 \\ x_3 \end{bmatrix}$$

while for the remaining 6 variables a single time constant dynamic has been selected to model their temporal evolution. The non-linear relations included in the propagation matrix impose the implementation of an extended Kalman filter (EKF) so that in each iteration cycle the differential equations are linearized around the state estimate calculated in the previous step. On the other side, the adoption of direction cosines, beyond preserving a more physical interpretation of trajectories of parameters, offers the further advantage of having a linear sensitivity

matrix that relates the 6 available measurements (y) to the states.

$$(12) \begin{bmatrix} y_1 \\ y_2 \\ y_3 \\ y_4 \\ y_5 \\ y_6 \end{bmatrix} = \begin{bmatrix} g \cdot S_A & 0 & 0 & 0 & 0 & 0 & 0 & 0 & 0 \\ 0 & g \cdot S_A & 0 & 0 & 0 & 0 & 0 & 0 & 0 \\ 0 & 0 & g \cdot S_A & 0 & 0 & 0 & 0 & 0 & 0 \\ 0 & 0 & 0 & S_G & 0 & 0 & 1 & 0 & 0 \\ 0 & 0 & 0 & 0 & S_G & 0 & 0 & 1 & 0 \\ 0 & 0 & 0 & 0 & 0 & S_G & 0 & 0 & 1 \end{bmatrix} \times \begin{bmatrix} x_1 \\ x_2 \\ x_3 \\ x_4 \\ x_5 \\ x_6 \\ x_7 \\ x_8 \\ x_9 \end{bmatrix}$$

We have also introduced an hybrid switching mechanism, as suggested by Rehbinder^[15], putting a threshold on the modulus of measured acceleration. When total acceleration is considerably higher than gravity, the measurement noise variance associated to accelerometers is switched from the real (datasheet) value to a much higher one, diverting the filter confidence only on gyros, as long as such a high dynamical state persists.

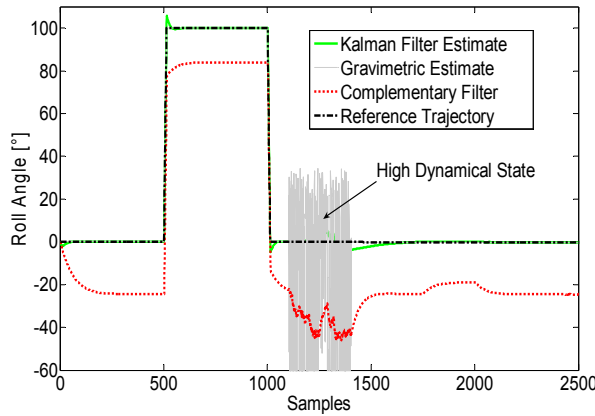


FIG 7. Simulation for comparison of the performances of different filters. The applied roll step has an amplitude of 100° and the slope of its edges is equal to the maximum angular rate of 400°/s.

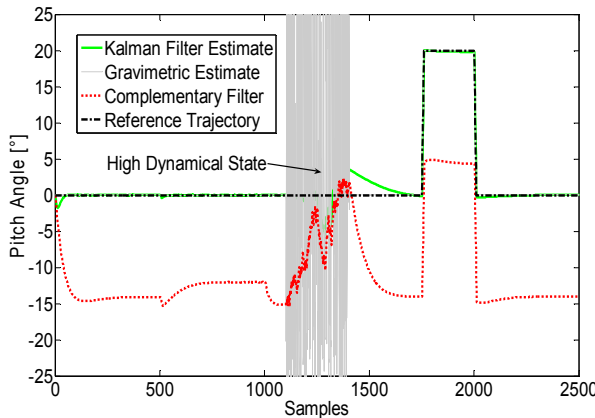


FIG 8. The applied pitch step has an amplitude of 20°, the slope is 400°/s and sampling period is 20ms.

The final critical issue consists in the tuning of filter parameters (covariance matrix, evolution time constants, switching threshold). Coarse tuning has been executed via simulations, while fine tuning requires real flight data that will be recorded in the future. The Matlab / Simulink simulation of FIG 7 and FIG 8 and shows a comparison of the performances of the 9-state Kalman filter vs. a high-pass + low-pass complementary filter, in response to roll and pitch steps and in presence of high dynamic spurious accelerations. The complementary filter offers the advantages of reduced computational burden and easier tuning procedure, having few parameters to be tuned (cut-off frequencies). This filter preserves a more direct relation to spectral behavior but is prone to the fundamental trade-off between response time and noise rejection. On the other side, the time-variant Kalman filter reaches a much better transient response (for the same noise rejection in high dynamical state) and no static error.

4. EXPERIMENTAL CHARACTERIZATION

4.1. Measurement Set-up

A demo system composed by both subunits has been realized, as shown in FIG 9 and FIG 10. Both boards interface to a PC on which a dedicated visual C software controls data acquisition and elaboration. Kalman filter routines have been developed in Matlab.

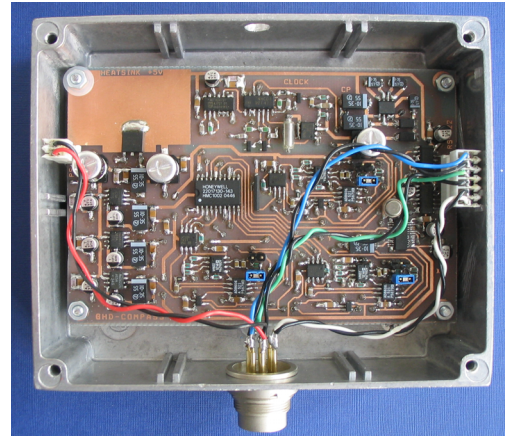


FIG 9. Compass demo unit.



FIG 10. Cluster of attitude sensors.

All tests have been executed indoor with standard electronic instrumentation and particular equipment: graduated precision mechanical rotating supports, a

calibrated platform and a climatic chamber. The bandwidth of cluster of attitude sensors is 100Hz and the time constant of the compass response is 50ms, 5 times faster than the visualization dynamic. Thus, there is margin for further low-pass filtering, that is unnecessary due to excellent resolution already demonstrated.

4.2. Resolution

Angular resolution has been tested by means of hand-operated rotating mechanical supports, applying angular steps of about 0.1° as illustrated in FIG 11 and FIG 12. It's evident that the resolution is much better than 0.1° for both heading and attitude as noise standard deviation is smaller than 0.05° . This achievement confirms the benefits of accurate low-noise electronic front-end design.

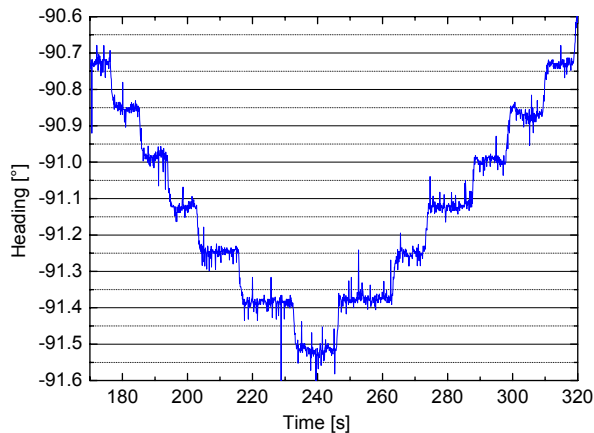


FIG 11. Heading angular resolution test: response to applied rotary steps of about 0.1° .

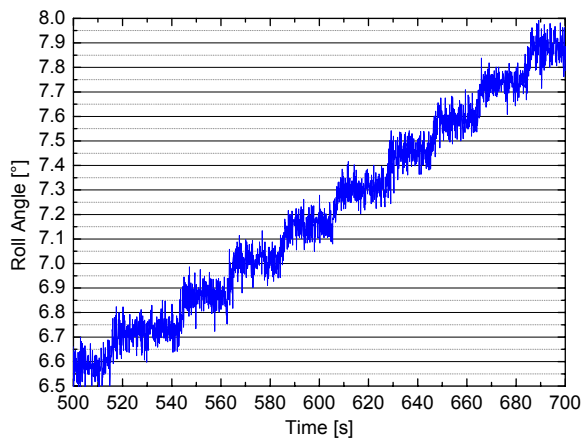


FIG 12. Roll angular resolution test: steps of about 0.1° .

4.3. Static Accuracy: Thermal Stability

The measurements executed over the entire thermal operating range confirm the necessity of adopting particular configurations that enable the achievement of complete fulfilment of specifications for both subsystems, as evident from the following plots. In particular from FIG 13, it's clear that closed-loop operating mode is successfully effective in reducing the total heading variation to less than 0.1° .

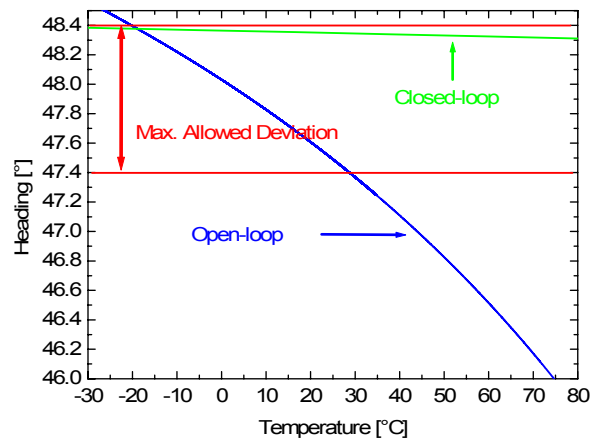


FIG 13. Heading thermal drift: open-loop vs. closed-loop

The expected improvement of accelerometer thermal drift has been experimentally verified. The differential approach guarantees that temperature-induced attitude variations stay well within the desired $\pm 0.5^\circ$ accuracy range as illustrated in the following plots.

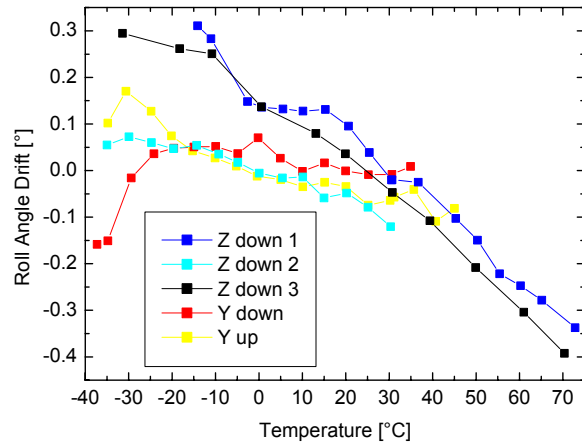


FIG 14. Roll thermal drift for various 3D orientations.

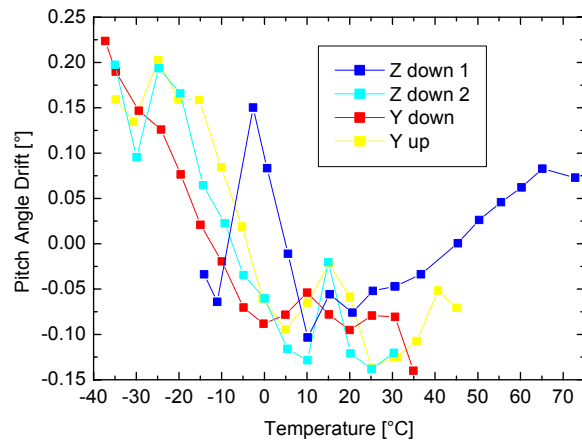


FIG 15. Pitch thermal drift in different 3D orientations.

Data plotted in FIG 14 and FIG 15 has been recorded in

various measurement sessions and for different 3D assembly orientations, aiming at testing the drift behavior in different sensor working points. The thermal drift of the differential configuration has resulted, in the worst case, equal to $38\mu\text{V}/^\circ\text{C}$, that is 15 times smaller than the single sensor drift.

4.4. Static Accuracy: Calibration

As already mentioned, the static calibration procedure of the attitude subunit is composed by two steps: offset nulling of accelerometers at room temperature and misalignment correction. To obtain the offset is sufficient to execute a complete rotation around each axis and calculate the mean of the measured sinusoid. In our demo-system under test, the residual static error after subtraction of measured values of offset (1.9mV, 8.7mV and -0.65mV) resulted still larger than specifications for roll angle, as visible in FIG 17 and FIG 18 (triangle).

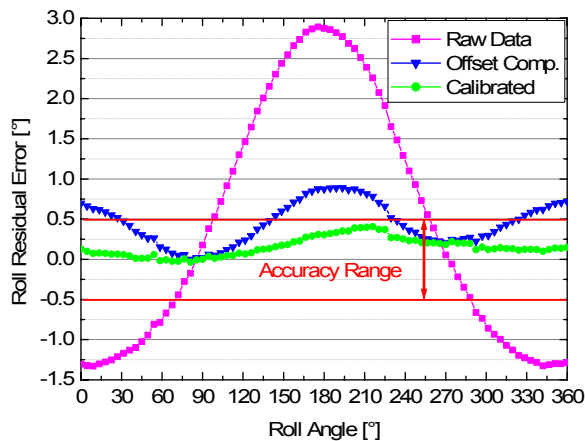


FIG 16. Roll residual static error after two calibration steps: offset compensation and misalignment calibration.

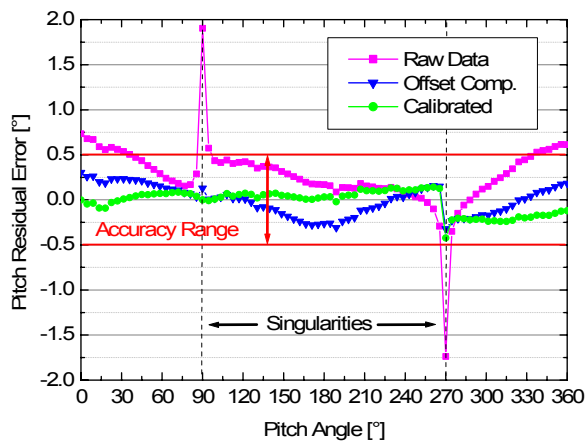


FIG 17. Pitch residual static error after two calibration steps: offset compensation and misalignment calibration.

The second step consists in the correction for misalignments of sensors and non orthogonal board mounting. Nine measurements, executed on a levelled platform that enables controlled rotations of exactly 90° , are necessary to obtain the 3×3 direction cosines matrix

that maps 6 acquired values to the ideal orthogonal and aligned triad. As shown in the graphs (circles) after such calibration both residual static errors are reduced within $\pm 0.5^\circ$.

In order to simulate a swinging procedure in laboratory, we sampled 12 known headings in presence of iron structures and recorded the error. The angular error function is well fitted (FIG 18) by a second order Fourier polynomial whose 5 coefficients were obtained through least squares. The residual heading error is so effectively reduced to $\pm 0.3^\circ$.

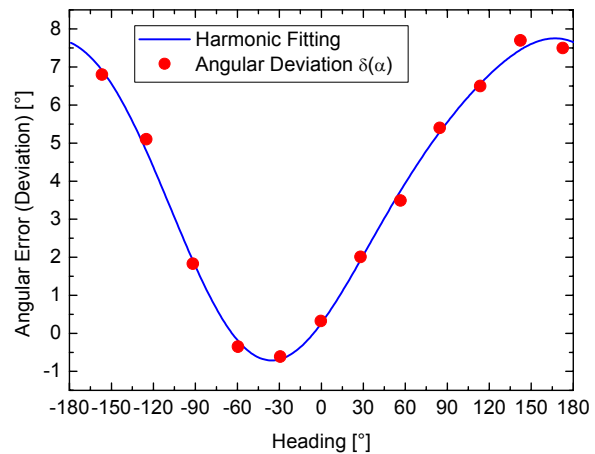


FIG 18. Heading iron distortion induced error (dots) and harmonic fitting function.

5. CONCLUSIONS

We have described the steps of the design process of an AHRS to be incorporated in state of the art ESIS, from the very beginning of solid state sensors selection to the construction of a fully-operating demo system, trying to point out fundamental critical issues that are common to the development of any attitude determination system.

The laboratory experimental characterization has demonstrated very good fulfillment of static performance requirements, confirming the importance of careful design, together with accurate calibration procedures. In particular, the adoption of lock-in filtering and closed-loop magnetic feedback for the compass and differential configuration for accelerometers has enabled the achievement of 0.1° angular resolution and 0.5° static accuracy over the entire thermal operating range. Flight tests have been programmed to assay dynamical performances in comparison with other commercial equipments.

Future developments include the realization of the air data computer, the integration of all systems into a common and properly selected digital elaboration platform.

6. ACKNOWLEDGEMENTS

We are indebted to Gianpiero Mastinu for his kind help. We want also to thank Ferruccio Francescotti, Vinicio Chiaverini, Valerio Cattani, Cesare Cardani, Alberto Folchini and Alberto Rolando for fruitful discussions.

7. REFERENCES

- [1] M. Kayton and W. Fried, Avionics Navigation Systems, II Ed. John Wiley & Sons, New York 1997
- [2] ARINC Specification No. 408A, "Air transport indicator cases and mounting", Aeronautical Radio, Inc. December 15, 1976
- [3] PNI Corporation, www.pnicorp.com, International Patent: G01R 33/02, G01C 17/00, 17/28
- [4] P. de Jong, F. Riedijk, and J. an der Meer, "Smart Silicon Sensors: Examples of Hall-Effect Sensors", Sensors 2002, Proceedings of the IEEE, Vol. 2, pp. 1440-1444, 12-14 June 2002
- [5] S. Kawahito, C. Maier, M. Schneider, M., Zimmermann and H. Baltes, "A 2-D CMOS Microfluxgate Sensor System for Digital Detection of Weak Magnetic Fields", *IEEE J. Solid-State Circuits*, Vol. 34, pp. 1843-1851, September 1999
- [6] S. Andreev and P. Dimitrova, "Anisotropic-Magnetoresistance Integrated Sensors", *Journal of Optoelectronics and Advanced Materials*, Vol. 7, pp. 199-206, No. 1, February 2005
- [7] M. Caruso, "Application of Magnetoresistive Sensors in Navigation Systems", *Sensors and Actuators* 1997, SAE SP-1220, pp. 15-21, February 1997
- [8] T. McGuire and R. Potter, "Anisotropic Magnetoresistance in Ferromagnetic 3d Alloys", *IEEE Trans. on Magnetism*, Vol. 11, No. 4, July 1975
- [9] Honeywell, "Set/Reset Function for Magnetic Sensors", Application Note AN213, 2002 www.magneticsensors.com
- [10] J. Kuipers, Quaternions and Rotation Sequences, Princeton University Press, Princeton 1999
- [11] D. Gebre-Egziabher, R. Hayward, and J. Powell, "Design of Multi-Sensor Attitude Determination Systems", *IEEE Trans. on Aerospace and Elect. Sys.*, Vol. 4, No 2, pp. 624-648, April 2004
- [12] J. Rohac, "Accelerometers and Aircraft Attitude Evaluation", Procs. of IEEE Sensors 2005, Irvine USA
- [13] G. Wahba, Problem 65-1, *SIAM Review*, Vol. 8, N° 3, 384-386, July 1966
- [14] M. Grewal and A. Andrews, Kalman Filtering: Theory and Practice Using Matlab, Wiley, 2001
- [15] H. Rehbinder and X. Hu, "Drift-Free Attitude Estimation for Accelerated Rigid Bodies", Procs. of the 2001 IEEE Int. Conf. on Robotics & Automation, Seoul, Korea, May 21-26, 2001